Article

MRI Detection and Therapeutic Enhancement of Ferumoxytol Internalization in Glioblastoma Cells

Michael S. Petronek [1,*], Nahom Teferi [2], Chu-Yu Lee [3], Vincent A. Magnotta [3] and Bryan G. Allen [1,*]

[1] Department of Radiation Oncology, University of Iowa, Iowa City, IA 52242, USA
[2] Department of Neurosurgery, University of Iowa, Iowa City, IA 52242, USA; nahom-teferi@uiowa.edu
[3] Department of Radiology, University of Iowa, Iowa City, IA 52242, USA; vincent-magnotta@uiowa.edu (V.A.M.)
* Correspondence: michael-petronek@uiowa.edu (M.S.P.); bryan-allen@uiowa.edu (B.G.A.); Tel.: +1-319-356-8019 (M.S.P. & B.G.A.); Fax: +1-319-335-8039 (M.S.P. & B.G.A.)

Abstract: Recently, the FDA-approved iron oxide nanoparticle, ferumoxytol, has been found to enhance the efficacy of pharmacological ascorbate ($AscH^-$) in treating glioblastoma, as $AscH^-$ reduces the Fe^{3+} sites in the nanoparticle core. Given the iron oxidation state specificity of T2* relaxation mapping, this study aims to investigate the ability of T2* relaxation to monitor the reduction of ferumoxytol by $AscH^-$ with respect to its in vitro therapeutic enhancement. This study employed an in vitro glioblastoma MRI model system to investigate the chemical interaction of ferumoxytol with T_2* mapping. Lipofectamine was utilized to facilitate ferumoxytol internalization and assess intracellular versus extracellular chemistry. In vitro T_2* mapping successfully detected an $AscH^-$-mediated reduction of ferumoxytol (25.6 ms versus 2.8 ms for FMX alone). The T_2* relaxation technique identified the release of Fe^{2+} from ferumoxytol by $AscH^-$ in glioblastoma cells. However, the high iron content of ferumoxytol limited T2* ability to differentiate between the external and internal reduction of ferumoxytol by $AscH^-$ (ΔT_2* = +839% for external FMX and +1112% for internal FMX reduction). Notably, the internalization of ferumoxytol significantly enhances its ability to promote $AscH^-$ toxicity (dose enhancement ratio for extracellular FMX = 1.16 versus 1.54 for intracellular FMX). These data provide valuable insights into the MR-based nanotheranostic application of ferumoxytol and $AscH^-$ therapy for glioblastoma management. Future developmental efforts, such as FMX surface modifications, may be warranted to enhance this approach further.

Keywords: ferumoxytol; glioblastoma therapy; glioblastoma imaging; pha

1. Introduction

Ferumoxytol (Feraheme®, FMX) is a clinically available, superparamagnetic iron oxide nanoparticle approved for treating iron deficiency anemia in patients with chronic kidney disease [1–4]. FMX can generate T1-contrast enhancement in tumor tissue in glioma imaging due to its ferromagnetic properties. FMX is a superparamagnetic iron oxide nanoparticle (SPION) with a Fe_3O_4 core that is about 30 nm in size, has a neutral charge, and resides within a carboxylated polymer coating [5]. Many units of the Fe_3O_4 core exist in one nanoparticle yielding a wide range of molecular weights with an average of about 730 kDa [6]. Because of the large iron content of one molecule of FMX (1 molecule has $\approx$ 5900 iron atoms or 1 nM FMX $\approx$ 5.9 µM iron), it can function as a T_1/T_2* MRI contrast agent [7,8]. Ferumoxytol's iron content and ferromagnetic properties also allow its use as a T_2*-contrast agent because T_2* relaxation times are largely influenced by paramagnetic and ferromagnetic materials (e.g., iron). FMX's superparamagnetic properties alter T_2* relaxation times [9,10]. FMX is an attractive MR contrast agent because it has a significantly longer intravascular half-life ($t_{1/2} \approx$ 14–21 h) than gadolinium-based compounds ($t_{1/2} \approx$ 1 h) [7,11].

Beyond its utility as an MRI contrast agent, FMX has shown potential as an anti-cancer therapy [12,13]. The anti-cancer mechanism of FMX has been suggested to be due to its redox activity. It has previously been shown that the Fe_3O_4 core can be oxidized by ionizing radiation, showing that FMX can serve as a reserve of redox-active iron [14]. FMX also reacts with H_2O_2 stimulating the release of iron from the nanoparticle. Thus, FMX may undergo redox reactions with a wide array of species. Ascorbate ($AscH^-$) is a one-electron reductant that can readily reduce some complexes of ferric (Fe^{3+}) to ferrous (Fe^{2+}) iron [15]. $AscH^-$ can reduce and release Fe^{2+} from ferritin, a Fe^{3+}-containing biological macromolecule that is the primary mechanism for intracellular iron storage [16–18]. Recently, it has been reported that $AscH^-$ catalyzes the decomposition of the FMX Fe_3O_4 core [19]. The chemical interaction between FMX and $AscH^-$ can be characterized by a significant reduction in FMX size ($\approx$66% reduction in 24 h), a release of redox-active Fe^{2+} that follows Michaelis–Menton kinetics, and a significant increase in H_2O_2 generation. The decomposition of FMX by $AscH^-$ was reported to enhance glioblastoma cell killing and importantly, the enhanced toxicity of FMX and $AscH^-$ was glioblastoma specific, as no significant in vitro toxicity was observed in normal human astrocytes [19]. Thus, the chemical pairing of FMX and $AscH^-$ represents a novel therapeutic strategy. However, the utility of FMX as an MRI contrast agent suggests that FMX and $AscH^-$ may have nanotheranostic potential.

T_2^* relaxation mapping is a quantitative MRI technique used primarily to indicate total iron content [20]. This technique is widely applicable clinically for cardiac and hepatic iron overload [21–26]. Recent studies have shown that beyond total iron content, T_2^* can provide information on the oxidation state of iron, specificity differentiating between Fe^{3+} and Fe^{2+} [27,28]. This effect is theorized to result from proton– electron dipole–dipole interactions associated with the number of unpaired electrons (i.e., electron spin magnetic moment) of transition metals [29]. Moreover, a recent phase 2 clinical trial testing $AscH^-$ therapy in combination with radiation and temozolomide showed that patients with short T_2^* relaxation times (i.e., high iron content) had significantly greater therapy responses [30]. Because T_2^* relaxation appears to be largely dependent on the paramagnetic properties of metals and can detect alterations in these electronic spin properties (e.g., reduction/oxidation of iron), T_2^* mapping may serve as a useful tool in the evaluation of FMX redox chemistry. Therefore, changes in T_2^* relaxation may be reflective of the disruption of the FMX Fe_3O_4 core by $AscH^-$. This study aims to provide detailed proof-of-concept insights into the ability of T_2^* mapping to evaluate Fe_3O_4 disruptions by $AscH^-$ with respect to the in vitro toxicity of extracellular and intracellular FMX.

2. Materials and Methods

2.1. Cell Culture

Commercially available and validated U87, U251, and U118 glioblastoma cells were cultured in DMEM-F12 media (15% FBS, 1% penicillin-strep, 1% Na-pyruvate, 1.5% HEPES, 0.1% insulin, and 0.02% fibroblast growth factor) and grown to 70–80% confluence at 21% O_2 before experimentation. Cells were treated for 1 h with $AscH^-$ (20 pmol cell^{-1}; $\approx$8–10 mM), diluted from a 1 M stock of $AscH^-$ in H_2O with pH = 7, in complete cell culture media without FBS or Na-pyruvate to prevent scavenging of H_2O_2. Cells were treated with 100 µM deferoxamine mesylate salt (DFO; Sigma, St. Louis, MO, USA; D9533) from a 110 mM stock in H_2O. FMX was used from the commercially available Feraheme$^{®}$ (30 mg mL^{-1} stock in saline).

2.2. In Vitro MRI Studies

Glioblastoma cells were treated with 20 pmol cell^{-1} $AscH^-$ for 1 h with 20 µg mL^{-1} FMX or pre-incubated for 24 h with 20 µg mL^{-1} FMX-L prior to the 1 h $AscH^-$ treatment. Following treatment, cells were trypsinized, re-suspended in sterile PBS, and transferred to PCR wells embedded in a 1% agarose gel phantom. Cells were allowed to collect at the bottom of the PCR well to form a pellet to be imaged. Cell pellets were then imaged on a 7T GE MR901 small animal scanner, a part of the small animal imaging core at the

University of Iowa. T_2* weighted images were collected using a gradient-echo sequence (TR = 10 ms, TE = 2.2, 8.2, 14.2, and 20.2 ms, matrix = 256 × 256, FOV = 25 × 20 mm, 2 signal averages). A B_0 shimming routine was performed to limit the effect of macroscopic field inhomogeneities. T_2* maps were generated using a combination of 4 echo times collected and fitting each voxel to a mono-exponential curve using in-house Python code. Images were imported to 3D Slicer software (V5.0.3) where regions of interest (ROIs) were delineated as a 1 mm diameter cylinder in the center of the tube and mean T_2* values were calculated using the label statistics tool within 3D Slicer [31].

2.3. FMX Internalization with Lipofectamine

Lipofectamine FMX (FMX-L) was generated using the commercially available lipofectamine 3000 reagents (Thermofisher Scientific, Waltham, MA, USA; L3000015). Functionalization was completed by diluting FMX at 1:16 in 1% FBS containing DMEM-F12 media (1 mL) with 10 μL P3000 reagent, vortexing vigorously for 5 s, and then diluting the FMX/P3000 stock at 1:1 with lipofectamine 3000. The samples were incubated at room temperature for 15 min prior to utilization. FMX-L was generated new for every experiment. The cells were then treated with FMX-L for 24 h in 1% FBS containing DMEM-F12 medium. The cells were washed with 1X D-PBS prior to additional studies to remove extracellular FMX.

2.4. Quantitation of Intracellular Iron

Intracellular iron concentrations were validated colorimetrically following a 24 h treatment with either 20 μg mL^{-1} FMX or FMX-L using a ferrozine-based assay [32,33]. Following treatment, cells were washed with sterile PBS, trypsinized, and centrifuged at 1200 rpm for 5 min. The cell pellets were resuspended in 1X RIPA buffer (Sigma-Aldrich, St. Louis, MO, USA; R0278) and sonicated 3 × 10 s to lyse the cells. Cell lysis solution was then diluted 1:1 in 2.5 M glacial acetic acid pH = 4.5 with 5 mM ferrozine and 10 mM AscH$^-$. The sample and buffer mixture were centrifuged at maximum speed (14,000× g) for 10 min to remove protein aggregates. The supernatant (200 μL) was placed in a 96-well dish [33]. Ultraviolet-visible light (UV-Vis) spectroscopic measurements were performed using a 96-well plate reader. Fe^{2+} (ferrozine)$_3$ complex formation was monitored by analyzing absorbance at 562 nm. Fe^{2+} concentrations were determined using Beer's Law for absorbance at 562 nm (ε_{562} = 27,900 M^{-1} cm^{-1}) with a path length, of L = 0.55 cm (200 μL sample).

2.5. Cellular Iron Staining

To visualize the iron deposition following FMX treatment, cells were stained using a Prussian Blue technique using an iron staining kit (Abcam, Cambridge, U.K.; ab150674) using the manufacturer's protocol. Following treatment, cells were washed with 1X D-PBS and fixed with formalin for 5 min. The cells were then washed with distilled H_2O and incubated for 15 min with a 1:1 mixture of potassium ferrocyanide and 2% hydrochloric acid. After staining, cells were washed with distilled H_2O and stained for 5 min with a nuclear-fast red counterstain. Finally, cells were washed with distilled H_2O and allowed to dry. The cells were then imaged using a phase contrast microscope with a 40× objective lens.

2.6. Electron Paramagnetic Resonance Evaluation of FMX Concentrations in Cell Culture Media

The FMX concentrations were determined by measuring the peak-to-peak signal intensity of the EPR spectrum of the low-spin Fe_3O_4 complex at $g \approx 2$ as previously described [14]. Using a Bruker EMX spectrometer, the following scan parameters were used to collect spectra: center field = 3508.97 G, sweep width = 2000 G, frequency = 9.85 GHz, power attenuation = 18 dB, modulation frequency = 100 kHz, modulation amplitude = 0.7 G, with spectra being generated from a signal average of 2 scans with 2048 resolution. U87 cells were incubated for 24 h with 20 μg mL^{-1} FMX or FMX-L.

3. Results

3.1. In Vitro Oxidation State Specificity of T_2* Mapping

Before evaluating if T_2* mapping can detect FMX and AscH$^-$ chemistry, the in vitro oxidation state specificity of T_2* mapping was tested using a previously established MRI phantom model system [29]. It was observed that AscH$^-$ increased T_2* relaxation times in U87, U251, and U118 GBM cell lines by 7 ms, 17 ms, and 10 ms, respectively (Figure 1). This is consistent with the previously observed increase in T_2* relaxation times following a pharmacological ascorbate infusion in GBM subjects [27]. Moreover, the iron chelator deferoxamine (DFO) causes a decrease (U87 = -12 ms, U251 = -6 ms, and U118 = -18 ms) in T_2* relaxation times indicative of a paramagnetic shift as a result of ferrioxamine (DFO-Fe^{3+}) complex formation. This is consistent with the ability of DFO to bind and maintain Fe in the +3 oxidation state (Fe^{3+}) [34]. Thus, T_2* mapping can detect iron oxidation state changes associated with the oxidation when complexed by DFO or internally reduced by AscH$^-$.
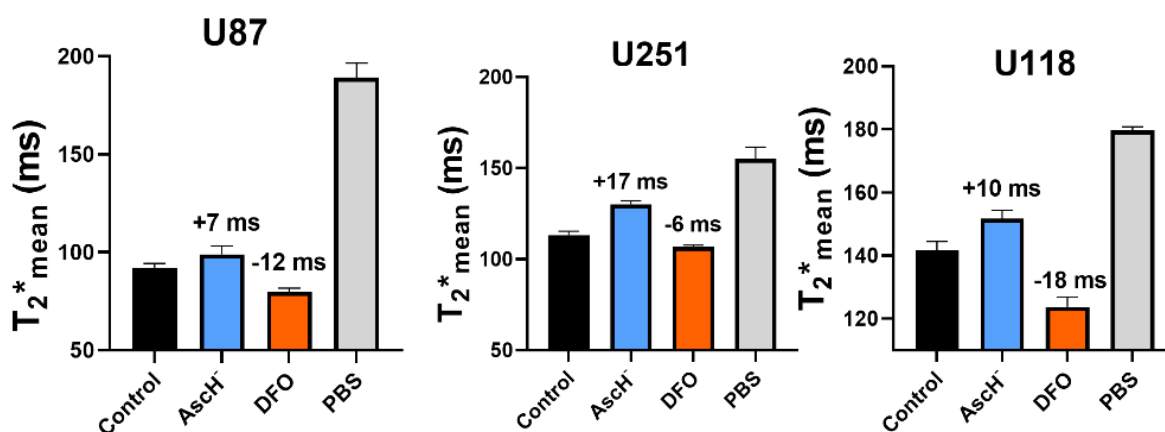

Figure 1. Pharmacological perturbations of intracellular iron can be detected in GBM cells using T_2* mapping. Quantification of in vitro T_2* maps of human GBM (U87, U251, U118) cells treated with P-AscH$^-$ (20 pmol cell^{-1}; range: 6–8 mM, 1 h) or DFO (200 μM, 24 h). Phosphate-buffered saline without cells was used as a positive control. Values represent the average magnitude of deflection in T_2* relaxation from control (n = 3).

3.2. Lipofectamine Enhances FMX Internalization

A potential limitation of this approach is the extracellular nature of FMX [35]. Therefore, a proof-of-concept internalization model using lipofectamine was used to determine if T_2* mapping can distinguish intracellular and extracellular FMX reduction by AscH$^-$. To validate this model system, U87 cells were incubated with 20 μg mL^{-1} FMX ± lipofectamine (FMX-L) for 24 h. The initial observation made using this approach was that cell pellets following treatment with FMX-L had a reddish hue that would be indicative of high iron content (Figure 2a). Quantitatively, there was a significant decrease in FMX concentrations in the cell culture media, evaluated using EPR spectroscopy (Figure 2b) [14]. This indicates a shift of FMX from the extracellular to the intracellular space. The cell pellets also showed a significant, ≥3-fold, increase in iron concentrations (Figure 2c). This was further validated using Prussian blue staining where intracellular iron was markedly increased following FMX-L treatment (Figure 2d). Interestingly, an increase in Prussian blue positive cells was visible following a 1 h FMX incubation. This effect was not as pronounced by 24 h. This suggests an initial extracellular accumulation of FMX that dissipates over time. Lipofectamine appears to be a valuable tool for facilitating FMX internalization and intracellular retention.
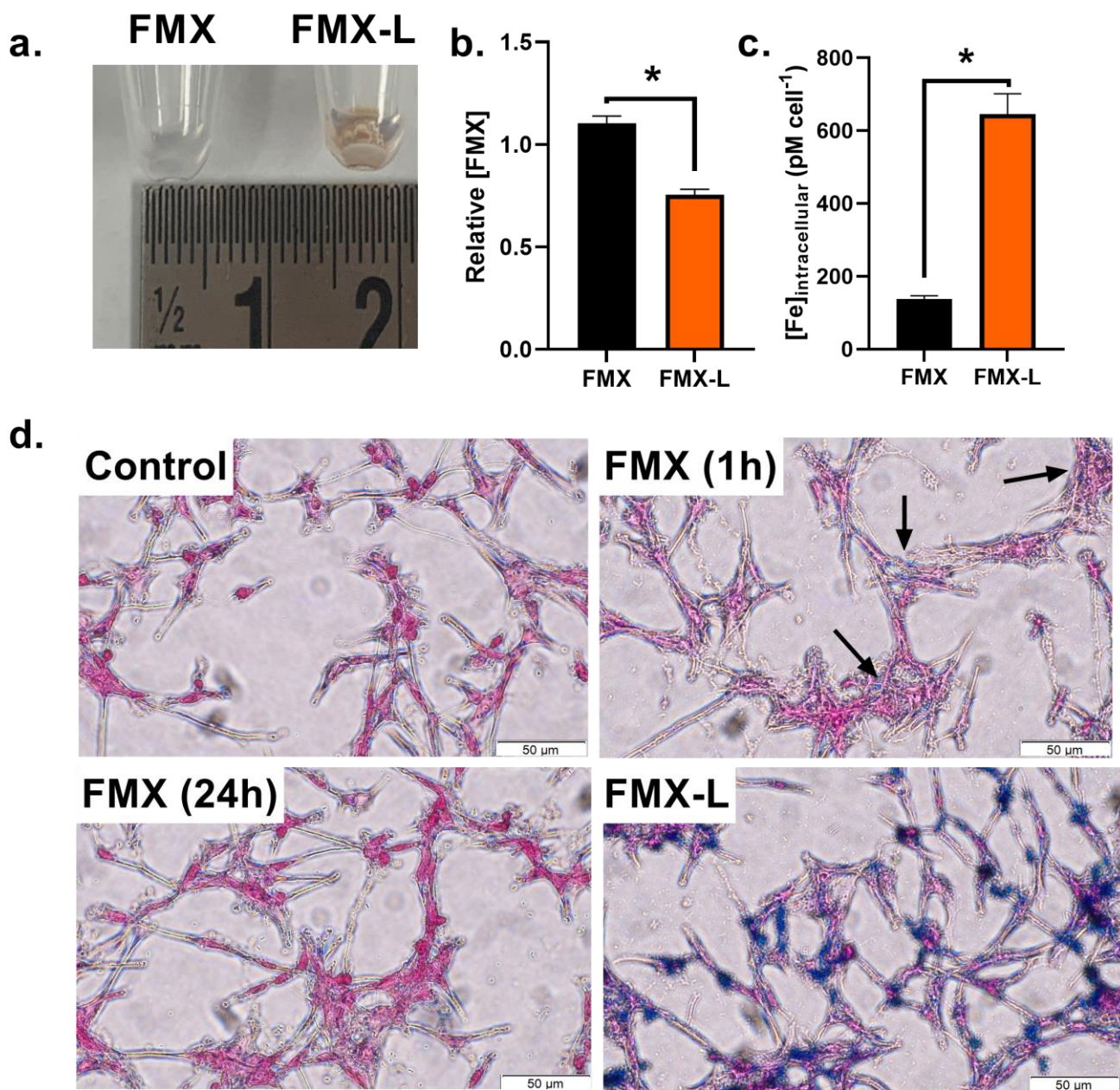
Figure 2. T_2* mapping detects FMX internalization and reduction in vitro. (**a**) Cells were treated for 24 h followed by PBS washing and trypsinization. The large increase in intracellular iron content of FMX-L becomes apparent due to the reddish hue of the cell pellet. (**b**) Relative [FMX] concentrations in cell culture media following 24 h incubation. This was done by evaluating the EPR spectral peak of FMX at t = 0 and t = 24 h and normalizing both FMX and FMX-L peaks to FMX alone. (**c**) Intracellular, chelatable iron content in U87 cells following a 24 h incubation with FMX or FMX-L. Error bars represent mean ± SEM with * $p < 0.05$ using a Welch's *t*-test. (**d**) Representative phase contrast (40×) Prussian blue images for cellular iron content in U87 cells treated with FMX for 1 h and 24 h, or 24 h FMX-L. Black arrows indicate clusters of Prussian blue-positive cells.

3.3. FMX Internalization Enhances AscH⁻ Cytotoxicity

This FMX internalization model system was used to evaluate if changes in T_2* relaxation times reflect the internal reduction of FMX by AscH⁻. U87 cells were either co-incubated for 1 h with 20 μg mL⁻¹ FMX ± 20 pmol cell⁻¹ AscH⁻ or pre-treated for 24 h FMX-L to load the cells with FMX prior to their 1 h AscH⁻ treatment. Following treatment, cells were pelleted for T_2* map generation. From this experiment, it has been observed that

following a 1 h treatment with FMX or a 24 h treatment with FMX-L caused a noticeable signal loss, likely due to the ferromagnetic properties of FMX (Figure 3a). In both FMX and FMX-L treated cells, there was an observable susceptibility artifact surrounding the cell pellet that was much larger in the FMX-L cells, indicative of the significant increases in intracellular iron content that were previously described. AscH$^-$-treated cells showed longer T_2* relaxation properties; however, this was difficult to qualitatively visualize in the FMX-L treated cells due to the large signal loss. Quantitatively, AscH$^-$ alone induced a 5 ms increase (control = 25.6 ms versus AscH$^-$ = 30.4 ms) in T_2 relaxation time, consistent with previous reports (Figure 3b) [27]. Both FMX and FMX-L cells caused a decrease in T_2* relaxation time to 2.8 and 1.9 ms, respectively. This is consistent with the observed FMX deposition with both treatments. In both cases (FMX and FMX-L), AscH$^-$ treated cells had significantly longer T_2* relaxation times (25.6 and 22.3 ms, respectively). The T_2* relaxation time change from baseline was significantly greater in those cells treated with FMX/FMX-L and AscH$^-$ than AscH$^-$ alone (Figure 3c). However, the internalization of FMX only partially increased the change in T_2* by AscH$^-$, suggesting that these doses of FMX for extracellular/intracellular differentiation were likely in the signal saturation range. Overall, these results further support the hypothesis that T_2* relaxation time can detect the reduction of FMX by AscH$^-$, but the high iron content of FMX may limit this effect.
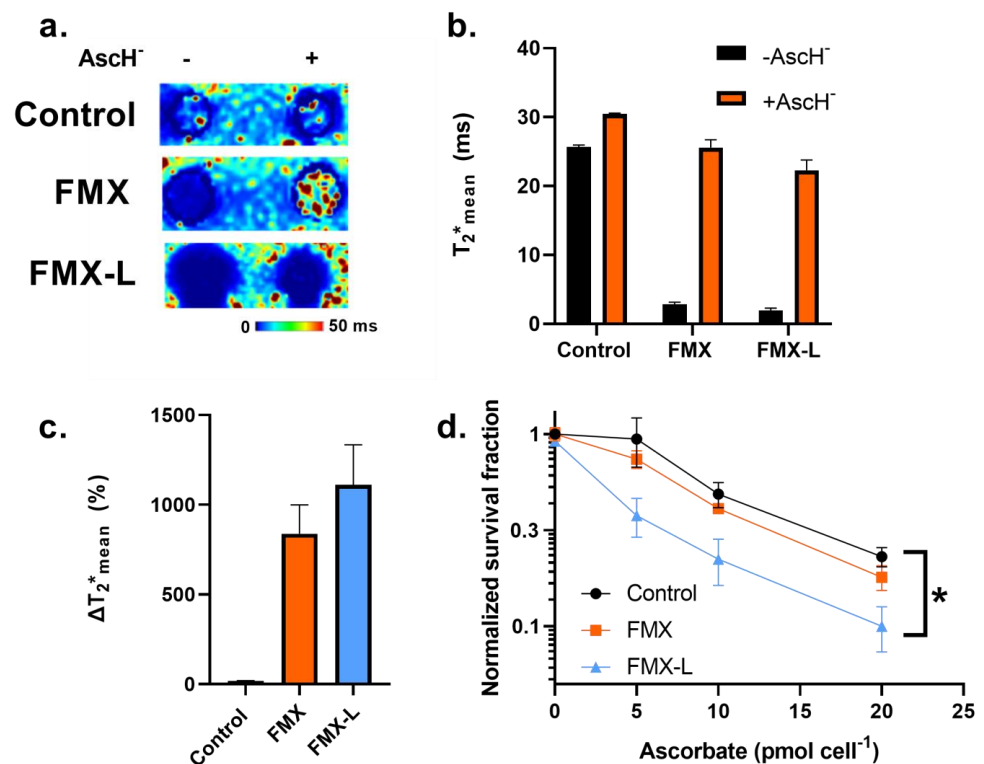

Figure 3. FMX internalization enhances AscH$^-$ cytotoxicity in glioblastoma cells. (**a**) Representative T_2* maps of U87 cell pellets treated with 20 pmol cell^{-1} AscH$^-$ ± standard 1 h co-incubation with 20 µg mL^{-1} FMX or 24 h pre-treatment with 20 µg mL^{-1} FMX-L. (**b**) Mean T_2* relaxation times in U87 cells treated with 20 pmol cell^{-1} AscH$^-$ ± standard 1 h co-incubation with 20 µg mL^{-1} FMX or 24 h pre-treatment with 20 µg mL^{-1} FMX-L. (**c**) Changes in T_2* relaxation time (% difference from untreated control) associated with 20 pmol cell^{-1} AscH$^-$ treatment standard 1 h co-incubation with 20 µg mL^{-1} FMX or 24 h pre-treatment with 20 µg mL^{-1} FMX-L. (**d**) Clonogenic dose–response curves for U87 cells treated with increasing concentrations of AscH$^-$ ± standard 1 h co-incubation with 20 µg mL^{-1} FMX or 24 h pre-treatment with 20 µg mL^{-1} FMX-L. Error bars represent mean ± SEM for three independent experiments with * $p < 0.05$ using a one-way ANOVA test with a post-hoc Tukey's test.

Moreover, it has recently been reported that the combination of FMX and AscH$^-$ exhibited enhanced cytotoxic effects in glioblastoma cells and significantly enhanced the standard of care therapy (radiation and temozolomide) in an in vivo animal model [19]. Thus, the therapeutic aspect of these imaging results was subsequently evaluated in glioblastoma cells. Based on the potential effects of FMX internalization on the ability of T$_2$* to detect nanoparticle reduction, the effects on AscH$^-$ toxicity were evaluated. Consistent with these imaging results, FMX-L significantly enhanced the dose-dependent AscH$^-$ toxicity in U87 cells as FMX had a dose-enhancement ratio of 1.16 ($p = 0.09$) as compared to 1.54 for FMX-L ($p < 0.05$; Figure 3d). Thus, it appears that the internalization of FMX represents a novel strategy to enhance its utility in combination with AscH$^-$; however, this may be a context-dependent effect that warrants further consideration.

4. Discussion

This study describes the ability of T$_2$* mapping to detect the release of ferrous iron from FMX by AscH$^-$. The primary utilization of FMX in the context of glioblastoma management is as an MR contrast agent [7,36,37]. FMX is also being investigated as a marker for glioblastoma progression [37]. Therefore, T$_2$* may also be a valuable tool to identify regions of FMX accumulation. We demonstrate that FMX can decrease T$_2$* relaxation times in vitro. This is consistent with previous data showing that FMX can decrease T$_2$* relaxation times in humans 24 h following its administration likely owing to its 14–21 h intravascular half-life [7,38]. In this study, supraphysiological concentrations of AscH$^-$ (10 mM), which are typically achieved via intravenous injection during glioblastoma therapy, were used [39,40]. Thus, this chemical combination more closely replicates an interaction that may be observed during glioblastoma therapy. Adding a reducing agent (AscH$^-$) to FMX increases T$_2$* relaxation times, which coincides with the release of Fe^{2+} from the nanoparticle core [19]. This is consistent with the iron oxidation state specificity of T$_2$* mapping [29]. The oxidation state specificity of T$_2$* mapping could be further validated in vitro in this study as AscH$^-$ induces an increase in T$_2$* relaxation while DFO causes a decrease. Importantly, this chemistry effect was able to be replicated in the context of AscH$^-$ and FMX chemistry as the addition of AscH$^-$ can prolong FMX relaxation times. This indicates that AscH$^-$ can reduce the Fe^{3+} sites of FMX leading to an increase in the Fe^{2+}:Fe^{3+} ratio, which can be detected with T$_2$* mapping. These results are consistent with the increase in T$_2$* associated with adding AscH$^-$ to FMX in an orthotopic glioblastoma model [19]. Thus, the present study provides further insights into the ability of T$_2$* mapping to detect the catalyzed release of Fe^{2+} from the Fe$_3$O$_4$ core by AscH$^-$.

FMX and AscH$^-$ chemistry was detected in both the extracellular and intracellular space with FMX internalization facilitated by lipofectamine. In this cell culture model, adding FMX caused a significant decrease in T$_2$* regardless of its localization. The internalization did appear to shorten T2* relaxation times further, consistent with the significant increase in cellular iron content; however, detectable differences were challenging due to potential signal saturation. In both cases, FMX and FMX-L, adding AscH$^-$ significantly increased T$_2$* relaxation times. Following the internalization of FMX (FMX-L), the increase in T$_2$* relaxation time induced by AscH$^-$ was slightly greater but was ultimately limited by the potential signal saturation caused by FMX. Thus, it is important to note that due to the large size ($\approx$30 nm) and high iron content of FMX, T$_2$* relaxation appears to lose the ability to detect intracellular versus extracellular localization [19,41]. Therefore, the use of T$_2$* may have an intrinsic technical limitation where the high iron concentrations of FMX limit the range of oxidation state specificity and impair the ability to evaluate FMX reduction by AscH$^-$. This can be overcome by using ultrashort echo time (UTE)-T$_2$* and may warrant further investigation [42].

Furthering the nanotheranostic potential of FMX and AscH$^-$, the internalization of FMX significantly enhanced AscH$^-$ toxicity. Thus, the internalization of FMX may significantly enhance the therapeutic utility in combination with AscH$^-$ in GBM. Developmental efforts have been previously put forth to functionalize FMX and enhance tumor traffick-

ing and internalization. For example, it has been shown that FMX functionalized with a Toll-like receptor 3 agonist enhanced melanoma tumor control [43]. Moreover, the trend towards a greater increase in T_2* relaxation following internalization suggests that FMX reduction by $AscH^-$ is driving the enhanced toxicity. These results are also consistent with previous literature that demonstrates increases in intracellular iron content enhance $AscH^-$ toxicity [44]. This would support the hypothesis that cellular $AscH^-$ uptake by sodium vitamin C transporters (SVCTs) mediate $AscH^-$ toxicity in glioblastoma cells [45]. Therefore, it can be hypothesized that surface modifications of FMX to increase tumor trafficking and internalization can enhance the effectiveness of FMX and $AscH^-$ in the management of GBM and warrant further investigation.

5. Conclusions

In summary, this study provides important insights into the utility of T_2* mapping as a tool for assessing FMX and $AscH^-$ chemistry in a biologically relevant model system. The large size of FMX can cause T_2* signal saturation in GBM cells, limiting the ability to detect FMX internalization robustly. However, the oxidation state specificity of T_2* mapping was partially retained. Moreover, the internalization of FMX significantly enhanced $AscH^-$ toxicity in glioblastoma cells. Thus, FMX internalization strategies (e.g., surface modifications) may warrant further investigation as a therapeutic approach. These data help contextualize the nanotheranostic application of FMX and $AscH^-$ therapy in glioblastoma to be considered in ongoing studies.

Author Contributions: Conception and design: M.S.P., V.A.M. and B.G.A.; Data collection and analysis: M.S.P., N.T. and C.-Y.L.; Data curation: M.S.P. and B.G.A.; Writing and editing: M.S.P., N.T., C.-Y.L., V.A.M. and B.G.A. All authors have read and agreed to the published version of the manuscript.

Data Availability Statement: Data is available upon request of the corresponding authors.

Conflicts of Interest: The authors declare no conflicts of interest.

References

1. Macdougall, I.C.; Strauss, W.E.; Dahl, N.V.; Bernard, K.; Li, Z. Ferumoxytol for Iron Deficiency Anemia in Patients Undergoing Hemodialysis. The FACT Randomized Controlled Trial. *Clin. Nephrol.* **2019**, *91*, 237–245. [CrossRef] [PubMed]
2. Rosner, M.; Bolton, W. Ferumoxytol for the Treatment of Anemia in Chronic Kidney Disease. *Drugs Today* **2009**, *45*, 779–786. [CrossRef]
3. Rosner, M.H.; Auerbach, M. Ferumoxytol for the Treatment of Iron Deficiency. *Expert. Rev. Hematol.* **2011**, *4*, 399–406. [CrossRef] [PubMed]
4. Auerbach, M.; Chertow, G.M.; Rosner, M. Ferumoxytol for the Treatment of Iron Deficiency Anemia. *Expert Rev. Hematol.* **2018**, *11*, 829–834. [CrossRef]
5. Bullivant, J.P.; Zhao, S.; Willenberg, B.J.; Kozissnik, B.; Batich, C.D.; Dobson, J. Materials Characterization of Feraheme/Ferumoxytol and Preliminary Evaluation of Its Potential for Magnetic Fluid Hyperthermia. *Int. J. Mol. Sci.* **2013**, *14*, 17501–17510. [CrossRef]
6. Balakrishnan, V.S.; Rao, M.; Kausz, A.T.; Brenner, L.; Pereira, B.J.G.; Frigo, T.B.; Lewis, J.M. Physicochemical Properties of Ferumoxytol, a New Intravenous Iron Preparation. *Eur. J. Clin. Investig.* **2009**, *39*, 489–496. [CrossRef]
7. Toth, G.B.; Varallyay, C.G.; Horvath, A.; Bashir, M.R.; Choyke, P.L.; Daldrup-Link, H.E.; Dosa, E.; Finn, J.P.; Gahramanov, S.; Harisinghani, M.; et al. Current and Potential Imaging Applications of Ferumoxytol for Magnetic Resonance Imaging. *Kidney Int.* **2017**, *92*, 47–66. [CrossRef]
8. Manning, P.; Daghighi, S.; Rajaratnam, M.K.; Parthiban, S.; Bahrami, N.; Dale, A.M.; Bolar, D.; Piccioni, D.E.; McDonald, C.R.; Farid, N. Differentiation of Progressive Disease from Pseudoprogression Using 3D PCASL and DSC Perfusion MRI in Patients with Glioblastoma. *J. Neuro-Oncol.* **2020**, *147*, 681–690. [CrossRef]

9. Iv, M.; Samghabadi, P.; Holdsworth, S.; Gentles, A.; Rezaii, P.; Harsh, G.; Li, G.; Thomas, R.; Moseley, M.; Daldrup-Link, H.E.; et al. Quantification of Macrophages in High-Grade Gliomas by Using Ferumoxytol-Enhanced MRI: A Pilot Study. *Radiology* **2019**, *290*, 198–206. [CrossRef]

10. McCullough, B.J.; Kolokythas, O.; Maki, J.H.; Green, D.E. Ferumoxytol in Clinical Practice: Implications for MRI. *J. Magn. Reson. Imaging* **2013**, *37*, 1476–1479. [CrossRef]

11. Weinstein, J.S.; Varallyay, C.G.; Dosa, E.; Gahramanov, S.; Hamilton, B.; Rooney, W.D.; Muldoon, L.L.; Neuwelt, E.A. Super-paramagnetic Iron Oxide Nanoparticles: Diagnostic Magnetic Resonance Imaging and Potential Therapeutic Applications in Neurooncology and Central Nervous System Inflammatory Pathologies, a Review. *J. Cereb. Blood Flow. Metab.* **2010**, *30*, 15–35. [CrossRef] [PubMed]

12. Trujillo-Alonso, V.; Pratt, E.C.; Zong, H.; Lara-Martinez, A.; Kaittanis, C.; Rabie, M.O.; Longo, V.; Becker, M.W.; Roboz, G.J.; Grimm, J.; et al. FDA-Approved Ferumoxytol Displays Anti-Leukaemia Efficacy against Cells with Low Ferroportin Levels. *Nat. Nanotechnol.* **2019**, *14*, 616–622. [CrossRef] [PubMed]

13. Zanganeh, S.; Hutter, G.; Spitler, R.; Lenkov, O.; Mahmoudi, M.; Shaw, A.; Pajarinen, J.S.; Nejadnik, H.; Goodman, S.; Moseley, M.; et al. Iron Oxide Nanoparticles Inhibit Tumour Growth by Inducing Pro-Inflammatory Macrophage Polarization in Tumour Tissues. *Nat. Nanotechnol.* **2016**, *11*, 986–994. [CrossRef] [PubMed]

14. Petronek, M.S.; Spitz, D.R.; Buettner, G.R.; Allen, B.G. Oxidation of Ferumoxytol by Ionizing Radiation Releases Iron. An Electron Paramagnetic Resonance Study. *J. Radiat. Res.* **2022**, *63*, 378–384. [CrossRef]

15. Buettner, G.; Anne Jurkiewicz, B. Catalytic Metals, Ascorbate and Free Radicals: Combinations to Avoid. *Radiat. Res.* **1996**, *145*, 532–541. [CrossRef] [PubMed]

16. Badu-Boateng, C.; Naftalin, R.J. Ascorbate and Ferritin Interactions: Consequences for Iron Release in Vitro and in Vivo and Implications for Inflammation. *Free. Radic. Biol. Med.* **2019**, *133*, 75–87. [CrossRef]

17. Badu-Boateng, C.; Pardalaki, S.; Wolf, C.; Lajnef, S.; Peyrot, F.; Naftalin, R.J. Labile Iron Potentiates Ascorbate-Dependent Reduction and Mobilization of Ferritin Iron. *Free. Radic. Biol. Med.* **2017**, *108*, 94–109. [CrossRef]

18. Harrison, P.M.; Arosio, P. The Ferritins: Molecular Properties, Iron Storage Function and Cellular Regulation. *Biochim. Biophys. Acta Bioenerg.* **1996**, *1275*, 161–203. [CrossRef]

19. Petronek, M.S.; Teferi, N.; Caster, J.M.; Stolwijk, J.M.; Zaher, A.; Buatti, J.M.; Hasan, D.; Wafa, E.I.; Salem, A.K.; Gillan, E.G.; et al. Magnetite Nanoparticles as a Kinetically Favorable Source of Iron to Enhance GBM Response to Chemoradiosensitization with Pharmacological Ascorbate. *Redox Biol.* **2023**, *62*, 102651. [CrossRef]

20. Chavhan, G.B.; Babyn, P.S.; Thomas, B.; Shroff, M.M.; Haacke, E.M. Principles, Techniques, and Applications of T2*-Based MR Imaging and Its Special Applications. *Radiographics* **2009**, *29*, 1433–1449. [CrossRef]

21. Anderson, L.; Holden, S.; Davis, B.; Prescott, E.; Charrier, C.; Bunce, N.; Firmin, D.; Wonke, B.; Porter, J.; Walker, J.; et al. Cardiovascular T2-Star (T2*) Magnetic Resonance for the Early Diagnosis of Myocardial Iron Overload. *Eur. Heart J. Cardiovasc. Imaging* **2001**, *22*, 2171–2179. [CrossRef] [PubMed]

22. Pepe, A.; Pistoia, L.; Martini, N.; De Marchi, D.; Barison, A.; Maggio, A.; Giovangrossi, P.; Bulgarelli, S.; Pasin, F.M.; Sarli, R.; et al. Detection of Myocardial Iron Overload with Magnetic Resonance By Native T1 and T2* Mapping Using a Segmental Approach. *Blood* **2018**, *132*, 2346. [CrossRef]

23. Henninger, B.; Kremser, C.; Rauch, S.; Eder, R.; Zoller, H.; Finkenstedt, A.; Michaely, H.J.; Schocke, M. Evaluation of MR Imaging with T1 and T2* Mapping for the Determination of Hepatic Iron Overload. *Eur. Radiol.* **2012**, *22*, 2478–2486. [CrossRef]

24. Wood, J.C. Magnetic Resonance Imaging Measurement of Iron Overload. *Curr. Opin. Hematol.* **2007**, *14*, 183–190. [CrossRef]

25. Wood, J.C.; Enriquez, C.; Ghugre, N.; Tyzka, J.M.; Carson, S.; Nelson, M.D.; Coates, T.D. MRI R2 and R2* Mapping Accurately Estimates Hepatic Iron Concentration in Transfusion-Dependent Thalassemia and Sickle Cell Disease Patients. *Blood* **2005**, *106*, 1460–1465. [CrossRef] [PubMed]

26. Ghugre, N.R.; Enriquez, C.M.; Gonzalez, I.; Nelson, M.D., Jr.; Coates, T.D.; Wood, J.C. MRI Detects Myocardial Iron in the Human Heart. *Magn. Reson. Med.* **2006**, *56*, 681–686. [CrossRef] [PubMed]

27. Cushing, C.M.; Petronek, M.S.; Bodeker, K.L.; Vollstedt, S.; Brown, H.A.; Opat, E.; Hollenbeck, N.J.; Shanks, T.; Berg, D.J.; Smith, B.J.; et al. Magnetic Resonance Imaging (MRI) of Pharmacological Ascorbate-Induced Iron Redox State as a Biomarker in Subjects Undergoing Radio-Chemotherapy. *Redox Biol.* **2021**, *38*, 101804. [CrossRef]

28. Birkl, C.; Birkl-Toeglhofer, A.M.; Kames, C.; Goessler, W.; Haybaeck, J.; Fazekas, F.; Ropele, S.; Rauscher, A. The Influence of Iron Oxidation State on Quantitative MRI Parameters in Post Mortem Human Brain. *NeuroImage* **2020**, *220*, 117080. [CrossRef]

29. Petronek, M.S.; St-Aubin, J.J.; Lee, C.Y.; Spitz, D.R.; Gillan, E.G.; Allen, B.G.; Magnotta, V.A. Quantum Chemical Insight into the Effects of the Local Electron Environment on T2*-Based MRI. *Sci. Rep.* **2021**, *11*, 20817. [CrossRef]

30. Petronek, M.S.; Monga, V.; Bodeker, K.L.; Kwofie, M.; Lee, C.-Y.; Mapuskar, K.A.; Stolwijk, J.M.; Zaher, A.; Wagner, B.A.; Smith, M.C.; et al. Magnetic Resonance Imaging of Iron Metabolism with T_2* Mapping Predicts an Enhanced Clinical Response to Pharmacological Ascorbate in Patients with GBM. *Clin. Cancer Res.* **2023**. [CrossRef]

31. Fedorov, A.; Beichel, R.; Kalpathy-Cramer, J.; Finet, J.; Fillion-Robin, J.-C.; Pujol, S.; Bauer, C.; Jennings, D.; Fennessy, F.; Sonka, M.; et al. 3D Slicer as an Image Computing Platform for the Quantitative Imaging Network. *Magn. Reson. Imaging* **2012**, *30*, 1323–1341. [CrossRef] [PubMed]

32. Stookey, L. Ferrozine-A New Spectrophotometric Reagent for Iron. *Anal. Chem.* **1970**, *42*, 779–781. [CrossRef]

33. Abbasi, U.; Abbina, S.; Gill, A.; Bhagat, V.; Kizhakkedathu, J.N. A Facile Colorimetric Method for the Quantification of Labile Iron Pool and Total Iron in Cells and Tissue Specimens. *Sci. Rep.* **2021**, *11*, 6008. [CrossRef] [PubMed]

34. Kiss, T.; Farkas, E. Metal-Binding Ability of Desferrioxamine B. *J. Incl. Phenom. Mol. Recognit. Chem.* **1998**, *32*, 385–403. [CrossRef]

35. McConnell, H.L.; Schwartz, D.L.; Richardson, B.E.; Woltjer, R.L.; Muldoon, L.L.; Neuwelt, E.A. Ferumoxytol Nanoparticle Uptake in Brain during Acute Neuroinflammation Is Cell-Specific. *Nanomedicine* **2016**, *12*, 1535–1542. [CrossRef]

36. Vasanawala, S.S.; Nguyen, K.-L.; Hope, M.D.; Bridges, M.D.; Hope, T.A.; Reeder, S.B.; Bashir, M.R. Safety and Technique of Ferumoxytol Administration for MRI. *Magn. Reson. Med.* **2016**, *75*, 2107–2111. [CrossRef] [PubMed]

37. Neuwelt, E.A.; Várallyay, C.G.; Manninger, S.; Solymosi, D.; Haluska, M.; Hunt, M.A.; Nesbit, G.; Stevens, A.; Jerosch-Herold, M.; Jacobs, P.M.; et al. The Potential of Ferumoxytol Nanoparticle Magnetic Resonance Imaging, Perfusion, and Angiography in Central Nervous System Malignancy: A Pilot Study. *Neurosurgery* **2007**, *60*, 601–611, discussion 611–612. [CrossRef]

38. Stirrat, C.G.; Alam, S.R.; MacGillivray, T.J.; Gray, C.D.; Forsythe, R.; Dweck, M.R.; Payne, J.R.; Prasad, S.K.; Petrie, M.C.; Gardner, R.S.; et al. Ferumoxytol-Enhanced Magnetic Resonance Imaging Methodology and Normal Values at 1.5 and 3T. *J. Cardiovasc. Magn. Reason.* **2016**, *18*, 46. [CrossRef]

39. Petronek, M.S.; Wagner, B.A.; Hollenbeck, N.J.; Caster, J.M.; Spitz, D.R.; Cullen, J.J.; Buettner, G.R.; Allen, B.G. Assessment of the Stability of Supraphysiological Ascorbate in Human Blood: Appropriate Handling of Samples from Clinical Trials for Measurements of Pharmacological Ascorbate. *Radiat. Res.* **2019**, *191*, 491–496. [CrossRef]

40. Allen, B.G.; Bodeker, K.L.; Smith, M.C.; Monga, V.; Sandhu, S.; Hohl, R.; Carlisle, T.; Brown, H.; Hollenbeck, N.; Vollstedt, S.; et al. First-in-Human Phase I Clinical Trial of Pharmacologic Ascorbate Combined with Radiation and Temozolomide for Newly Diagnosed Glioblastoma. *Clin. Cancer Res.* **2019**, *25*, 6590–6597. [CrossRef]

41. Marashdeh, M.W.; Ababneh, B.; Lemine, O.M.; Alsadig, A.; Omri, K.; El Mir, L.; Sulieman, A.; Mattar, E. The Significant Effect of Size and Concentrations of Iron Oxide Nanoparticles on Magnetic Resonance Imaging Contrast Enhancement. *Results Phys.* **2019**, *15*, 102651. [CrossRef]

42. Hong, W.; He, Q.; Fan, S.; Carl, M.; Shao, H.; Chen, J.; Chang, E.Y.; Du, J. Imaging and Quantification of Iron-Oxide Nanoparticles (IONP) Using MP-RAGE and UTE Based Sequences. *Magn. Reson. Med.* **2017**, *78*, 226–232. [CrossRef] [PubMed]

43. Zhao, J.; Zhang, Z.; Xue, Y.; Wang, G.; Cheng, Y.; Pan, Y.; Zhao, S.; Hou, Y. Anti-Tumor Macrophages Activated by Ferumoxytol Combined or Surface-Functionalized with the TLR3 Agonist Poly (I:C) Promote Melanoma Regression. *Theranostics* **2018**, *8*, 6307–6321. [CrossRef] [PubMed]

44. Brandt, K.E.; Falls, K.C.; Schoenfeld, J.D.; Rodman, S.N.; Gu, Z.; Zhan, F.; Cullen, J.J.; Wagner, B.A.; Buettner, G.R.; Allen, B.G.; et al. Augmentation of Intracellular Iron Using Iron Sucrose Enhances the Toxicity of Pharmacological Ascorbate in Colon Cancer Cells. *Redox Biol.* **2018**, *14*, 82–87. [CrossRef]

45. Burgess, E.R.; Crake, R.L.I.; Phillips, E.; Morrin, H.R.; Royds, J.A.; Slatter, T.L.; Wiggins, G.A.R.; Vissers, M.C.M.; Robinson, B.A.; Dachs, G.U. Increased Ascorbate Content of Glioblastoma Is Associated With a Suppressed Hypoxic Response and Improved Patient Survival. *Front. Oncol.* **2022**, *12*, 829524. [CrossRef]